Case Studies in Thermal Engineering 76 (2025) 107444

Contents lists available at ScienceDirect

Case Studies in Thermal Engineering

journal homepage: www.elsevier.com/locate/csite

Using pin fins arrangements to improve melting heat and mass transfer in a cylindrical enclosure

Fathi Alimi [a], Abdul Amir H. Kadhum [b], Mohamed Bouzidi [c], Mohammed Hasan Ali [d], Hammadi Khmissi [e,*], Zehba Raizah [f], Faisal Alresheedi [g], Turki Alkathiri [h], D. Iranian [i,**]

[a] *Department of Chemistry, College of Science, University of Ha'il, P.O. Box 2440, Ha'il, 81441, Saudi Arabia*
[b] *University of Al-Ameed, Karbala, Iraq*
[c] *Department of Physics, College of Science, University of Ha'il, P.O. Box 2440, Ha'il, Saudi Arabia*
[d] *College of Technical Engineering, Imam Ja'afar Al-Sadiq University, Al-Muthanna, 66002, Iraq*
[e] *Department of Physics, College of Science, Northern Border University, Arar, 73213, Saudi Arabia*
[f] *Department of Mathematics, Faculty of Science, King Khalid University, Abha, Saudi Arabia*
[g] *Department of Physics, College of Science, Qassim University, Buraidah, 51452, Saudi Arabia*
[h] *Department of Electrical Engineering, College of Engineering, Al-Baha University, P.O. Box 65799, Albaha, Saudi Arabia*
[i] *Department of Mathematical Sciences, Saveetha School of Engineering, SIMATS, Chennai, 602105, Tamilnadu, India*

GRAPHICAL ABSTRACT

Thermal energy storage in cylindrical fins in a shell-tube cylindrical cylinder energy storage unit.

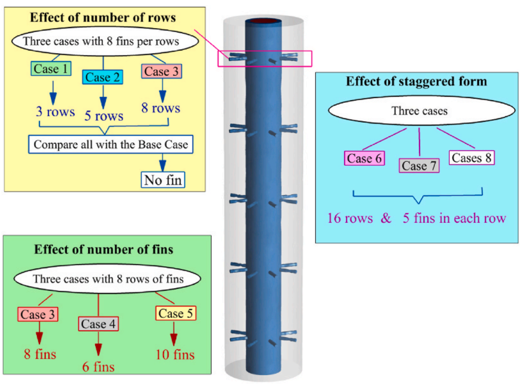

* Corresponding author.
** Corresponding author.
E-mail addresses: f.alimi@uoh.edu.sa (F. Alimi), amir1719@gmail.com (A.A.H. Kadhum), elbouzidimed16@yahoo.com (M. Bouzidi), mohammed.hasan@sadiq.edu.iq, mh180250@gmail.com (M.H. Ali), hammadi.ali@nbu.edu.sa (H. Khmissi), zaalrazh@kku.edu.sa (Z. Raizah), F.Alresheedi@qu.edu.sa (F. Alresheedi), turkialkathiri@bu.edu.sa (T. Alkathiri), iraniand.sse@saveetha.com (D. Iranian).

https://doi.org/10.1016/j.csite.2025.107444
Received 7 August 2025; Received in revised form 4 November 2025; Accepted 20 November 2025
Available online 21 November 2025

ARTICLE INFO

Keywords:
Melting heat transfer
Natural convection
Heat and mass transfer
Phase change material
Cylindrical fins

ABSTRACT

This study presents a numerical investigation of the melting behavior of RT35 phase change material (PCM) in latent heat thermal energy storage (LHTES) in the presence of pin fins. The influence of specific 3D arrangement of the pin fins on the heat and mass transfer and natural convection flows was addressed in a full 3D model of the enclosure including the phase change effects. The primary motivation for using cylindrical fins was to allow molten PCM to flow more freely through fin rows, enhancing natural convection. Results reveal that increasing the number of fin rows enhances conduction heat transfer but can obstruct natural convection flow in molten PCM, reducing convection and hindering overall efficiency. Optimizing the number of fin rows is critical to balancing these effects, achieving significant improvements in the heat transfer and energy storage performance. To mitigate the negative impact of increased fin rows on natural convection, staggered fin arrangements were introduced, leading to a 27.9 % reduction in melting time compared to the base case without fins. Additionally, the inline configuration provided a 29 % acceleration in heat transfer and PCM melting time compared to a base case. Cylindrical fins were 10.2 % better than disk fins.

1. Introduction

The pressing need to ensure sustainable energy practices has become a central focus in addressing the escalating global energy demand. As traditional energy resources pose numerous challenges, renewable energy has emerged as a viable alternative [1]. However, the inherent intermittency and supply-demand imbalance have highlighted the necessity for efficient energy storage systems [2].

Thermal Energy Storage (TES), particularly Latent Heat Thermal Energy Storage (LHTES) systems using Phase Change Materials (PCM), presents an effective solution for its energy density and stability of performance [3]. In an equal storage volume, LHTES can store roughly five to fourteen times more heat than sensible storage [4]. This makes it particularly suitable for applications in solar energy collection [5], building energy savings [6], reuse of industrial waste heat [7], and air conditioning [8]. However, one of the main limitations of LHTES is the poor thermal conductivity of most PCMs, which slows heat redistribution during melting and solidification. This limitation has spurred extensive research into heat transfer enhancement techniques such as using nanoencapsulation [9], metal foams [10], and fins [11]. Among these techniques, using fins as heat transfer surfaces has emerged as one of the most effective and widely studied methods [12–14]. Fins are a widely used passive technique that improves energy transfer in LHTES systems owing to their simple design, low cost, and effectiveness. Prior studies have covered classical longitudinal/annular fins [15–17] and a broad spectrum of bio-/math-inspired layouts (pin [18–20], spiral [21–23], branched [24], corrugated [25]), consistently showing a conduction–convection trade-off that must be balanced for fast charge/discharge. Recent evidence also shows high effectiveness from gradient tree-shaped fins and bionic (biomimetic) fins, which markedly shorten charge/discharge times [26,27].

Beyond cataloguing shapes, the primary objective of these studies is to reduce the solidification and melting times of PCM, making it more efficient as an energy storage medium. Rectangular or longitudinal fins are among the most commonly used configurations in LHTES systems. An experiment by Rathod and Banerjee [28] demonstrated that fins can reduce the solidification time by more than 74.8 %. According to Yuan et al. [29], fin installation angle affects PCM melting in a shell-tube LHTES, and fins installed near the bottom of a PCM container were more efficient at reducing melting time, illustrating the importance of fin placement.

Zhang et al. [30] investigated L-shaped fins in vertical enclosures and found the angle between the two sections had a significant influence on both melting and solidification. A 14 % reduction in melt time and a 45 % reduction in solidification time was found using optimal angles for these processes. Tiari et al. [31] experimentally investigated the effects of uniform and varying annular fin lengths on the thermal performance of a cylindrical LHTES system using RT-55 as the phase change material. Seven configurations with equal total fin volume were tested, including 10 fins (1.587 mm) and 20 fins (0.794 mm), each with uniform, increasing, or decreasing lengths. Results showed that fin geometry significantly affected charging and discharging rates. The configuration with 20 fins whose lengths increased toward the bottom achieved the highest improvement, providing the shortest charging and discharging times among all cases. This reflects section-wise heat-transfer characteristics of the storage system.

In cylindrical geometries, Oliveski et al. [32] examined horizontally embedded fins in a cavity in terms of their aspect ratio. PCM melting is accelerated by increasing fin length relative to thickness. The work of Farahani et al. [33] compared continuous and discrete fins in various shapes, including rectangular, annular, and spiral designs. Their findings emphasized that continuous fins, especially in rectangular shapes, significantly improved the liquid fraction of PCM during charging, with a 37.87 % increase compared to systems without fins. This improvement highlights the importance of maximizing the contact surface area between PCM and fins to enhance heating efficiency. It can be noted that active strategies, an elastic-driven phase-change thermal buffer and rapid charging/discharging protocols, can outperform traditional passive fins; however, their added complexity and actuation requirements limit adoption in building and solar LHTES applications, motivating our focus on passive fin optimization [34,35].

Innovative designs such as branched tree-like fins, as studied by Zhu and Jing [36], offer potential for optimizing LHTESS performance. Their research indicated that while increasing the angle or length of branches is not always beneficial to melting efficiency, there is an optimal configuration that maximizes heat transfer. Huang et al. [37] examined the use of sinusoidal-shaped fins, concluding that these fins were capable of enhancing solidification and melting in certain wave situations. Alimi et al. [38] explored the use of various fin configurations to enhance heat transfer in LHTES systems. They evaluated multiple fin configurations, including longitudinal, annular, and spiral fins, and analyzed their effects on thermal performance. The results demonstrated that the strategic placement of fins significantly improved heat transfer rates, thereby reducing the time required for PCM phase transitions and improving the overall efficiency of the LHTES systems. The study also highlighted the importance of optimizing fin geometries and material properties to maximize the thermal conductivity of the system. Similarly, Liu and Zhang [39] proposed a fin structure incorporating branching fins along an axial fin. Using this model, they demonstrated a reduction of 32.7 % in melting time and a reduction of 52.9 % in solidification time. Additionally, Shank et al. [40] found that axial fins of varying lengths, decreasing from bottom to top, significantly improved LHTESS efficiency, particularly during the melt process.

Xu et al. [41] developed metal fins with a memory function that reduce solidification and melting times by over 28 %. This adaptive approach illustrates the potential of dynamic fin designs in optimizing LHTESS performance under varying operating conditions. Moreover, the use of elliptical and Fibonacci-inspired fins has shown promise in enhancing heat transfer. An elliptical fin study conducted by Wang et al. [42] revealed that placing the ellipse vertically enhanced melt rate by 16.9 %. Baghaei et al. [43] explored Fibonacci-inspired fins, which improved PCM solidification and melt times by 45 % and 20 %, respectively, in comparison to longitudinal fins. These studies suggest that incorporating geometric inspiration from natural and mathematical patterns can lead to significant improvements in LHTES systems.

Gürtürk and Kok [44] further evaluated the role of fin surfaces on thermal transfer in vertical TES with different fin configurations. Their research revealed that a larger surface area of fins results in more efficient heat transfer during solidification and melting, particularly when natural convection effects are mitigated. This finding underscores the importance of designing fins that maximize surface area while maintaining effective buoyancy-driven flow. Additionally, Qianjun et al. [45] explored pointer-shaped fins, combining rectangular and triangular shapes, achieving a 64.2 % charging time reduction compared to bare tubes and a 15.1 % reduction compared to rectangular fins.

The present study offers a controlled 3-D comparison of cylindrical (pin) fin arrangements under an equal-fin-volume constraint, varying row count, per-row density, and staggering to isolate geometry effects from material addition. Keeping the mass of cylindrical fins constant is crucial to provide a fair analysis of the heat transfer advantage of phase change advantages. Despite extensive studies, a controlled 3-D comparison of cylindrical (pin) fin arrangements under an equal-fin-volume constraint, decoupling geometry from simple material addition, remains underexplored. While studies have examined the use fins for heat transfer enhancements in LHTES systems, most have focused on conventional fin geometries such as rectangular or longitudinal fins, with limited attention to alternative shapes like cylindrical fins. Additionally, many investigations have been conducted using two-dimensional models, which fail to capture the complex, three-dimensional nature of heat transfer in real-world applications. Furthermore, there are limited comprehensive researches comparing the capability of different configurations of cylindrical fins, particularly in terms of consideration the equal fins volume in all cases. This study addresses these gaps by investigating the impact of cylindrical configurations on phase change material melting behavior in a three-dimensional shell-tube LHTES system. Through a detailed numerical analysis, the study explores variations in fin geometry, number of rows, fin count, and staggered arrangements to identify the most efficient configurations while the fin mass (volume) is kept fixed. The results of this study provide practical design rules (row count, per-row density, and staggering) that balance conduction gains with buoyancy preservation, offering low-complexity guidance for building and solar LHTES. This work not only provides a deeper understanding of the role of fin design in heat transfer. It also compares the performance of different cylindrical fin configurations, offering new insights into the potential for improving energy storage systems.

2. Description and formulation of the model

2.1. The model's overview

Due to the intermittent nature of solar energy, which is only available during daylight hours, thermal energy storage is essential for ensuring a continuous supply of heat. One effective method is to use a LHTES unit, which stores solar energy in the form of latent heat using PCMs. In the system described, solar collectors heat water in a storage tank. An auxiliary cycle then circulates this hot water to the LHTES unit. When excess solar heat is available, the water temperature in the tank rises, and the auxiliary cycle charges the LHTES unit by transferring heat to the PCM, causing it to melt and store energy. Conversely, when solar heat is insufficient, the auxiliary cycle discharges the LHTES unit by circulating water through it, allowing the PCM to solidify and release the stored heat back to the water tank, thereby maintaining its temperature. While LHTES units can store large amounts of heat, the low thermal conductivity of PCMs limits the rate at which heat can be stored or released. To address this issue, thermal enhancement techniques are necessary. In this system, cylindrical fins are incorporated into the LHTES unit to improve heat transfer within the PCM, thereby increasing the efficiency of the storage process.

Fig. 2 illustrates the graphical design of the LHTES, comprising a container for the PCM equipped with rows of fins. The system features an inner cylinder that transports hot water flow (HWF) and is enclosed by an outer cylinder filled with PCM. Heat from the hot water passes through the copper tube wall and into the PCM; the fins enlarge the wetted area and guide heat into the bulk.

This study evaluates four distinct design configurations (as depicted in Fig. 1), focusing on how fin layout and tube placement affect system performance. The primary aim is to analyze how different fin configurations impact the overall performance of the system. The base configuration, referred to as the Base Case, lacks fins and operates with an inlet hot water velocity of $w_{i,HWF} = 0.0135$ m/ s, and an inlet temperature of $T_{i,HWF} = 323$ K. This serves as a baseline for comparing the effectiveness of various fin designs.

Table 1 presents eight different cylindrical fin configurations. Each maintains a constant total fin volume while varying the number of rows, fins per row, and fin diameter. The total volume of the fins for each configuration is calculated using the following equation:

$$V_{fins} = N_{fins}\left(\pi \frac{{D_{fin}}^2}{4} L_{fin}\right) \tag{1}$$

where D_{fin} and L_{fin} denote the diameter and length of the fins, and N_{fins} is the total number of fins, determined by the product of the number of rows and fins per row. Cases 1 through 3 explore the effects of varying the number of fin rows, while Cases 4 and 5 investigate the impact of changing the number of fins per row. Additionally, Cases 6 through 8 evaluate staggered fin arrangements to assess their influence on system performance.

Material thermophysical properties used in this analysis are summarized in Table 2. These include RT35 PCM (supplied by Rubitherm GmbH, Germany) as the medium for storing energy, water as the medium for transferring heat, and copper for the fins and tube walls. The properties considered, such as density, specific heat capacity, and thermal conductivity, were crucial in evaluating the system's heat transfer capabilities.

3. Formulating mathematically

The melting process of the PCM within a finned vertical shell-tube LHTES has been investigated based on energy-porosity theory [50]. To simplify the computational process, several assumptions are made [51,52]. The analysis assumes the flow is incompressible, laminar, and transient [53]. Additionally, the energy equation neglects viscous dissipation, and the thermophysical PCM properties are treated as temperature-independent over the narrow operating range (302–323 K), where typical variations in ρ, c_p, and k are small; the phase change itself is captured through the latent term and an l_f-weighted conductivity. Natural convection is accounted for by applying the Boussinesq approximation, while the PCM volume change during the phase transition is ignored. Solid PCM is assumed stationary (no breakup or sinking of solid fragments) and close-contact melting is not modeled; these mechanisms are associated with freely moving solids or elastically driven interfaces and lie outside the present fixed-container configuration [34].

The model considers both forced convection within the HWF inside the tubes and natural convection within the PCM chambers. Mass conservation for both HWF and PCM flows is governed as follows:

$$\frac{\partial U_j}{\partial x_j} = 0 \tag{2}$$

The momentum and energy conservation equations for HWF are as follows:

$$\rho_{HWF}\left(\frac{\partial U_i}{\partial t} + \frac{\partial (U_i U_j)}{\partial x_j}\right) = -\frac{\partial P}{\partial x_i} + \mu_{HWF}\frac{\partial}{\partial x_j}\left(\frac{\partial U_i}{\partial x_j} + \frac{\partial U_j}{\partial x_i}\right) \tag{3}$$

$$\frac{\partial T}{\partial t} + U_j \frac{\partial T}{\partial x_j} = \alpha_{HWF}\frac{\partial^2 T}{\partial x_j \partial x_j} \tag{4}$$

Here, the reference temperature T_{ref} is set at 293 K. $\boldsymbol{U}$ represents the average velocity, P stands for pressure, T stands for static temperature, t stands for flow time, β_{HWF} stands for water thermal expansion coefficient and α_{HWF} stands for water thermal diffusivity. The energy conservation equation for the intermediate thick copper walls is formulated as:

$$\frac{\partial T}{\partial t} = \alpha_{copper}\frac{\partial^2 T}{\partial x_j \partial x_j} \tag{5}$$

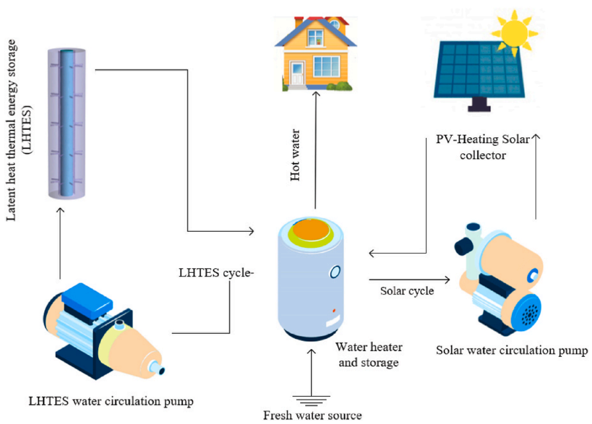

Fig. 1. LHTES in a solar heating cycle for providing hot water and heating to a building.

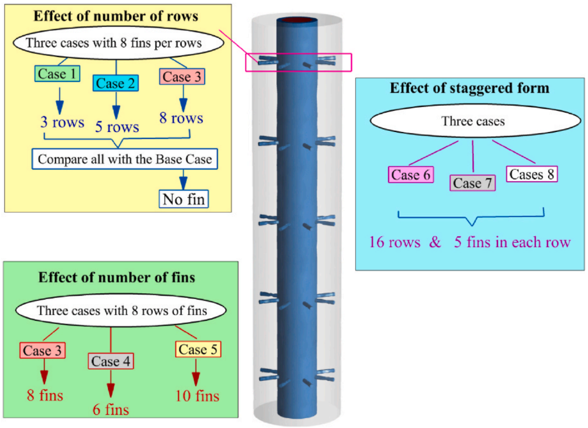

Fig. 2. Schematic of investigated cases with cylindrical fins through a cylindrical cylinder.

Table 1
Characteristics of cylindrical fin configurations.

Case	Number of Rows	Number of Fins/Rows	Staggered	Fin Diameter D_{fin} (mm)	Fin Length L_{fin} (mm)	Total Fin Volume (mm^3)
Case 1	3	8	No	2.58	10	1257
Case 1	5	8	No	2	10	1257
Case 3	8	6	No	1.83	10	1257
Case 4	8	8	No	1.58	10	1257
Case 5	8	10	No	1.41	10	1257
Case 6-8	16	5	Yes	1.41	10	1257

Table 2
Thermophysical properties of materials (water, RT35, and copper).

Material	Ref.	Properties						
		Density (kg/m^3)	Viscosity (kg/m. s)	Specific heat (J/kg. K)	Thermal conductivity (W/m. K)	Latent heat (kJ/kg)	Solidus temperature (°C)	Liquidus temperature (°C)
Water	[46]	997	0.000957	4179	0.613	–	–	–
RT35	[47, 48]	815	0.023	2000	0.2	160	32	38
Copper	[38, 49]	8978	–	387.6	381	–	–	–

Eq. (2) is valid for continuity of PCM in the domain. Besides, according to the Boussinesq approximation, the momentum equations for PCM flow are expressed as follows [54–56]:

$$\rho_{PCM}\left(\frac{\partial U_i}{\partial t}+\frac{\partial(U_iU_j)}{\partial x_j}\right)=-\frac{\partial P}{\partial x_i}+\mu_{PCM}\frac{\partial}{\partial x_j}\left(\frac{\partial U_i}{\partial x_j}+\frac{\partial U_j}{\partial x_i}\right)+\rho_{PCM}g_i\beta_{PCM}\left(T-T_{ref}\right)+S_i \tag{6}$$

To incorporate the effects of phase changes in convection, a damping term based on Darcy's law, also referred to as the source term, is introduced [57]:

$$S_i=\frac{\left(1-l_f\right)^2}{\left(\varepsilon+{l_f}^3\right)}U_iA_{mushy} \tag{7}$$

The constant A_{mushy} known as the mushy constant, usually lies between 10^5 Pa s/m^2 and 10^7 Pa s/m^2; for this study, it is assumed to be 10^5 Pa s/m^2 [58–60]. This value lies at the lower end of the standard range to avoid excessive artificial damping in semi-solid zones while still suppressing velocities in fully solid regions. Prior studies employing paraffin-based PCMs in similar enclosure geometries reported stable, experimentally consistent results with $A_{\rm mushy}=10^5$ Pa s/m^2 [58–60]. In our model, the selection is further supported by the validation in Fig. 6, where simulated temperature histories and FMV closely match experimental data, indicating that the chosen mushy constant does not bias the melt dynamics. Amount of ε is small (0.001) and it is used to prevent division by zero. The liquid fraction (l_f) is computed as follows:

$$l_f = \begin{cases} 0 \quad \text{if } T < T_{PCM_{solid}} \\ \dfrac{T - T_{PCM_{solid}}}{T_{PCM_{liquid}} - T_{PCM_{solid}}} T_{PCM_{solid}} < T < T_{PCM_{liquid}} \\ 1 \; T > T_{PCM_{liquid}} \end{cases} \tag{8}$$

The energy conservation for PCM flow is expressed as [55,56]:

$$\frac{\partial}{\partial t}(\rho_{PCM_m} H_T) + U_j \frac{\partial\left(\rho_{PCM_{Liquid}} H_T\right)}{\partial x_j} = \frac{\partial}{\partial x_j}\left(k_{PCM_m} \frac{\partial T}{\partial x_j}\right) \tag{9}$$

where H_T represents total volumetric enthalpy, resulting from the sum of sensible enthalpy (h_s) and latent heat (h_L) as follows:

$$H_T = h_s + h_L l_f \tag{10}$$

Moreover, l_f also influences thermophysical properties, such as thermal conductivity:

$$k_{PCM_m} = l_f k_{PCM_{Liquid}} + (1 - l_f) k_{PCM_{Solid}} \tag{11}$$

3.1. Boundary definitions

This geometry's boundary conditions are illustrated in Fig. 3. The HWF enters the system at a temperature of $T_{\mathrm{HWF,\,in}}$ and a velocity of $w_{HWF,\,in}$. At the outlet of the HWF tube, pressure outlet boundary conditions are applied. The enclosure's bottom, top, and sides walls are at zero heat flux, no-slip, and impermeable. The initial conditions assume a cold domain temperature of $T_{ref} = 293\mathrm{K}$, with $\mathbf{U} = 0$, and $\boldsymbol{P} = 0$. To compare different configurations, the fraction of melting volume (FMV) over time is used as the key performance indicator, which is computed by integrating the l_f over the entire domain.

4. Solver methodology

In the numerical approach, a pressure-velocity coupling method was applied to solve the Navier-Stokes equations. Gradients of variables were determined using the Cell-Based Least Squares approach. The QUICK scheme was employed for the discretization of both energy and momentum equations, while pressure correction was carried out using the PRESTO procedure.

Under-relaxation factors were set at 0.1 for momentum and pressure, and 0.6 for energy. Convergence thresholds were set at 10^{-4}, for both momentum and continuity equations, and 10^{-6}, for the energy equation. The model was considered complete when the phase change material fully melted, indicated by a melted volume fraction of 1. Additional details on the mesh study and validation can be found in the next section. Fig. 4 shows a flowchart of the applied computer code for the finite volume method.

5. Independency of the grid and validation

This section outlines the mesh sensitivity analysis and validation against previous experimental studies. To ensure numerical accuracy, both spatial and temporal convergence were assessed. For Case 2, which consists of five rows of fins with eight fins per row, and where the inlet hot water velocity w_{in_HWF} was 0.01345 m/s, and the inlet temperature T_{in_HWF} was 50°C, a mesh sensitivity study was

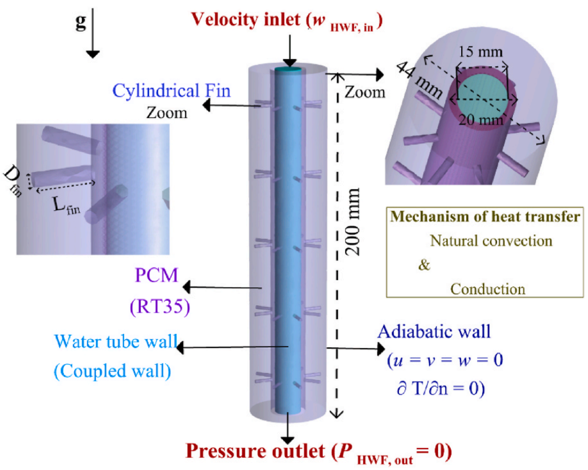

Fig. 3. Illustration of present open LHTES unit's boundary conditions.

performed. An unstructured mesh was used in the cylindrical fin and PCM domains, while a structured mesh was used in the HWF domain inside the tube and the tube wall. Meshes were refined near the walls to better capture temperature and fluid-flow gradients.

Fig. 5 presents the variation in the FMV as the number of mesh elements (CN) and the time step (ΔT) were adjusted. The results were repeated for several mesh sizes. As the mesh size reduces the number of required elements increases. The outcomes revealed some differences between very low element number of 190,000 and higher mesh numbers. There are minimal differences in FMV when the mesh size increased from 340,000 to 600,000 elements. As a result, 340,000 elements were used for the mesh size. Using this mesh size, a time step study has been performed. This choice follows a time-step sensitivity study (Fig. 5(b)): decreasing ΔT from 0.30–0.35 s–0.25 s produced indistinguishable FMV–time curves, while a further reduction to 0.15 s yielded no meaningful change in FMV or stored-energy trajectories. Therefore $\Delta T = 0.25$ s is adopted as a conservative time step that preserves temporal accuracy and stability at substantially lower computational cost.

5.1. Validating the data

Initially, the numerical model's accuracy was evaluated by comparing it with experiments [61]. These experiments examined the process of paraffin wax melting in an enclosed rectangular cavity 120 mm by 50 mm. Besides the left vertical wall, the cavity's walls were insulated. Several thermocouples measured temperature variations inside the cavity. Initially, the paraffin wax was at 25 °C, while the heated wall was set to 70 °C.

In the validation case, the computational domain reproduces the rectangular cavity (120 × 50 mm); the left wall is prescribed at T = 70 °C (Dirichlet), the other walls are adiabatic (Neumann), and the PCM is initially uniform at 25 °C. Natural convection arises under gravity with Boussinesq density variation. The phase change is captured with the same enthalpy–porosity formulation and A_{mushy} used in section 3; material properties match those reported in Ref. [61]. Performance metrics are (i) temperature-time histories at four midline points (T12, T21, T25, T30) and (ii) the time evolution of stored energy and FMV.

Fig. 6(a) shows the temperature distribution over time at four different points along a vertical line in the middle of the cavity,

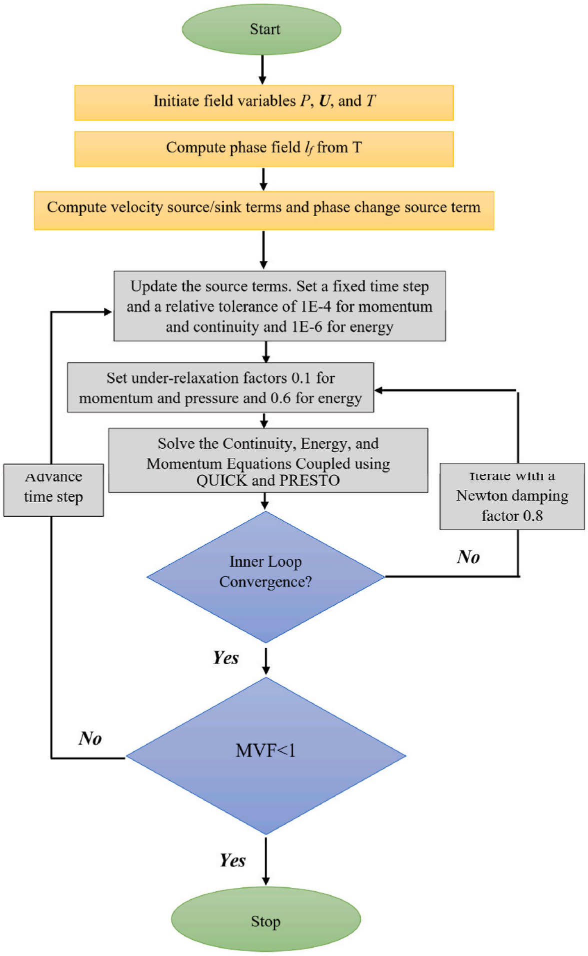

Fig. 4. A flowchart of the numerical code and the applied finite volume method.

comparing the experimental data with the simulated results from the current study. Additionally, Fig. 6(b) shows the amount of energy stored and FMV during the melt process. Agreement is good across all probes: the model captures the rapid warming after the onset of buoyancy and the subsequent approach to thermal equilibrium. Minor early-time deviations reflect sensor conduction lags and the absence of subcooling effects in the model; small late-time differences occur as the experimental system asymptotically approaches steady state while the simulation reaches FMV = 1 slightly earlier due to idealized boundary insulation. Overall, the predicted energy storage and FMV trends in Fig. 6(b) track the experimental curves closely, supporting the validity of the numerical model for the present parameter space.

To strengthen credibility for fin-assisted LHTES, experimental studies also are cited that investigated pin/cylindrical fins with paraffin PCMs, which report similar trends in the balance between added conduction area and preserved buoyant circulation. Arshad et al. [62] (round pin-fin heat sinks with PCM; enhanced melt rate), Mahmoud et al. [63] (triple-tube storage with circular/staggered fins; convection–conduction interplay), and Safari et al. [64] (comparative fin structures including pin fins) corroborate the mechanisms invoked in the results of this work, conduction benefits increase with fin area, but excessive alignment or blockage can suppress buoyancy and lengthen the melting tail.

6. Findings and discussion

This study explores the impact of several design parameters on the efficiency of a TES system. Key variables under investigation include the number of fin rows, the fin density per row, and the use of staggered fin configurations, all while ensuring consistent copper usage across the different setups. The discussion proceeds from geometry that primarily affects conduction capacity (total fin area) to geometry that governs the convection allowance (inter-row spacing and blockage), and it reports results consistently at intermediate FMVs (0.25, 0.50, 0.75) and near-complete melting (FMV = 0.95).

6.1. Effects of number of rows

The first step of this study investigates how varying the number of cylindrical fin rows affects the melting and storing efficiency in a TES. Three configurations—referred to as Cases 1-3—were designed, each with different numbers of rows but maintaining a constant eight fins per row. The comparison of the FMV and energy storage across these cases is illustrated in Fig. 7. Relative to the Base Case, all finned cases accelerate the initial melting (FMV = 0–0.3) because the added surface area increases conduction from the hot tube; however, high-row counts later slow the approach to FMV → 1 as buoyancy-driven circulation is restricted between closely spaced rows.

Based on Table 3, Case 2 (five rows of fins) showed the most improvement in melting time (t), reducing the total melting time by 29 % at an FMV of 0.95 compared to the Base Case. For intermediate FMVs of 0.25, 0.5, and 0.75, similar trends were observed, with Case 2 consistently outperforming the others. Case 1 (three rows) adds insufficient area and therefore exhibits minor gains, whereas Case 3 (eight rows) adds area but overly suppresses natural convection, so its benefit is smaller than Case 2.

Fig. 8 further compares the FMV contours of the Base Case with those of three scenarios at different intervals. Increasing the number of rows from three (Case 1) to five (Case 2) accelerated the melting process, while adding more rows (as in Case 3) hindered efficiency, despite having a larger surface area for heat transfer. The contours show stronger upward plumes and broader liquid regions in Case 2, evidencing more effective buoyancy circulation; in Case 3, liquid channels are thin and localized, indicating plume shielding by closely spaced rows.

This counterintuitive result can be explained by examining the melted PCM's movement. As shown in Table 4, Case 3 had a larger total fin surface area, yet the melting process was slower than Case 2. This was due to the limited mobility of the liquid PCM between the closely spaced fins, which restricted natural convection. In contrast, Case 2, with fewer rows, allowed more space for the melted PCM to circulate, enhancing natural convective heat transfer. The calculated effective volume (EV), defined as the space between the PCM and the first row of fins, also support this explanation. Larger EV and inter-row pitch in Case 2 promote "chimney" paths for

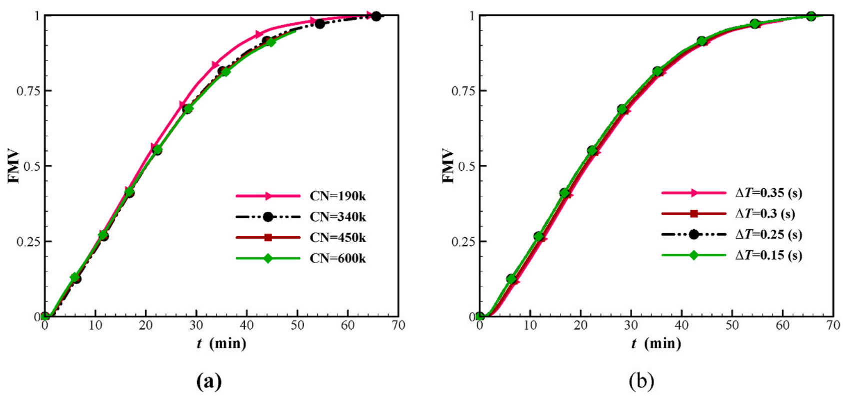

Fig. 5. Illustration of the influence of (a) mesh size and (b) time step on the precision of the FMV outcomes.

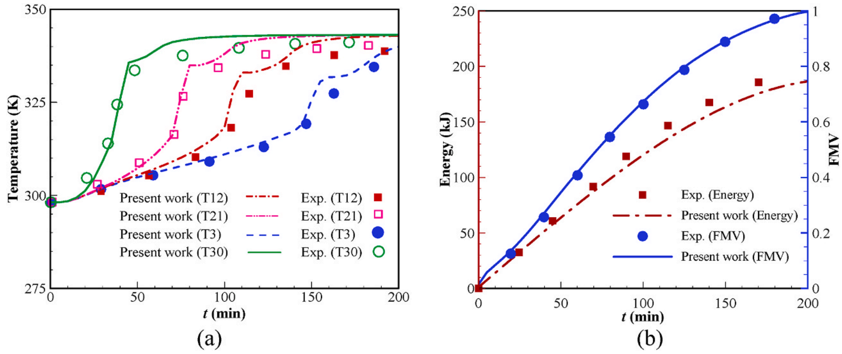

Fig. 6. A comparison between the current study and experimental [61] literature work: (a) temperature distribution as a function of time, (b) stored energy, and FMV.

buoyant plumes, increasing convective heat transport to downstream PCM. It can be concluded that, the optimum row count that balances conduction capacity (more area) with convection allowance (less blockage) in this geometry is five rows (Case 2).

Fig. 9 presents the change in temperature of both the solid components (tube and fins) and the PCM over time. There is a thermal boundary layer formed around the HWF wall and fins, with the temperature increasing in the upper part of the system due to the accumulation of melted PCM driven by natural convection. The fin row spacing plays a critical role in this process. In Case 2, the larger spacing between the fin rows allows the melted PCM to flow more freely, accelerating the melting process. In Case 1, the greater distance between rows results in less impact on melting, while in Case 3, the smaller spacing restricts the flow of the melted PCM, contributing to inefficient thermal transfer. These temperature fields corroborate the FMV trends in this way, Case 2 exhibits earlier top-zone warming and thicker high-T layers (stronger plumes), whereas Case 3 shows persistent stratification and late warming of the mid-height PCM (plume shielding).

6.2. *Fin number effects*

This phase of the investigation varied fin density per row at a fixed row count (eight rows) to isolate the role of per-row area and blockage. The total volume of fins was held constant across all configurations by adjusting the diameter of the fins. The configurations included Case 4 with six fins per row, Case 3 with eight fins, and Case 5 with ten fins per row. Fig. 10 illustrates the melting progress for each configuration over time, demonstrating that increasing the number of fins systematically improves the melting rate. Fig. 10 also shows the energy storage trends, where more fins per row lead to more efficient energy storage. The early-time slopes of FMV(t) increase with fin count (stronger conduction), while the late-time saturation (FMV → 1) is only mildly affected because inter-row spacing is unchanged. The FMV contours in Fig. 11 further highlight how fin density impacts melting processes. With 10 fins/row (Case 5) the liquid shells around each row expand and merge earlier, indicating higher local heat flux; with 6 fins/row (Case 4) the shells remain thinner and more isolated.

As summarized in Table 5, Case 5 exhibited the greatest reduction in melting time, achieving a 24.6 % decrease compared to the Base Case at an FMV of 0.95. This improvement was observed at all stages of the melting process (FMVs of 0.25, 0.5, 0.75, and 0.95).

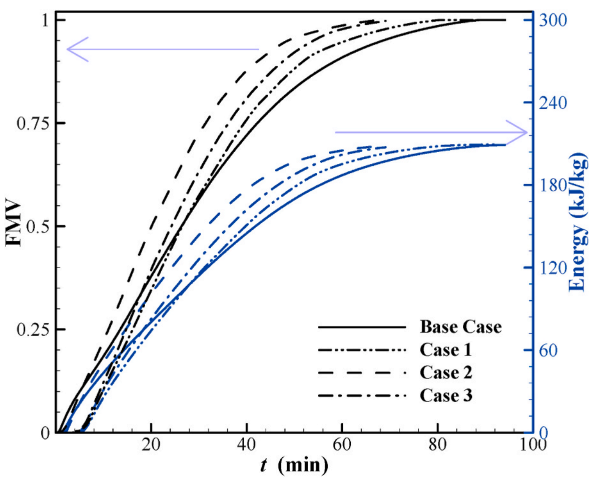

Fig. 7. Comparison of melting evolution profiles for Base Case (without fins), and Cases 1, 2, and 3.

Table 3
Melting time comparison and percentage change in melting time for cases 1, 2, and 3 relatives to the Base Case across four amounts of FMV.

Case	Number of rows	FMV = 0.25		FMV = 0.5		FMV = 0.75		FMV = 0.95	
		t (min)	Time change (%)	*t* (min)	Time change (%)	*t* (min)	Time change (%)	*t* (min)	Time change (%)
Base Case	–	13.54	–	26.37	–	42.25	–	68.56	–
Case 1	3	16.14	19.2	26.50	0.5	39.49	−6.5	60.96	−11.1
Case 2	5	11.06	−18.3	20.09	−23.8	31.42	−25.6	48.65	−29.0
Case 3	8	14.78	9.1	24.24	−8.1	36.20	−14.3	54.03	−21.2

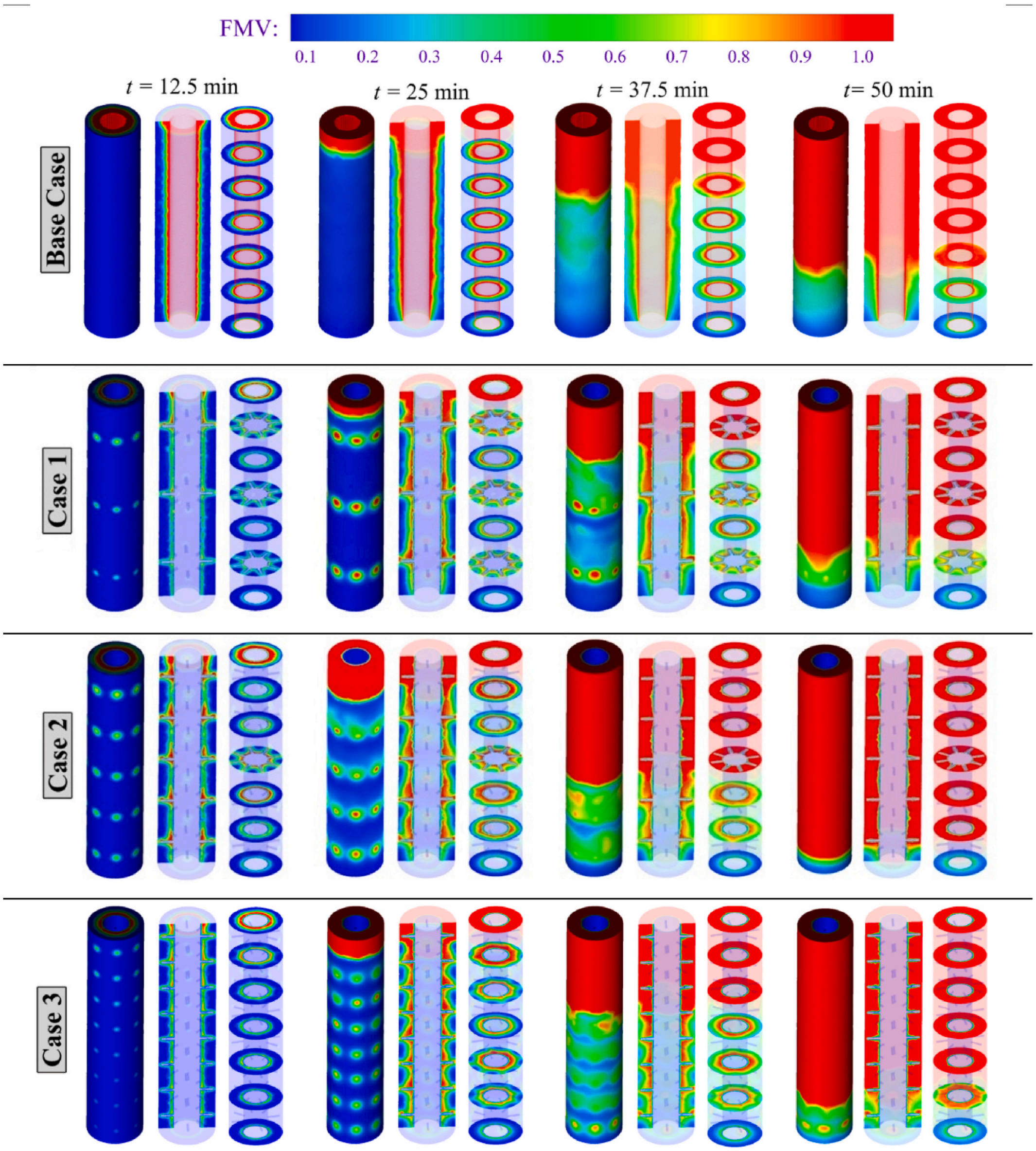

Fig. 8. FMV contour comparison for Base Case and Cases 1–3.

Case 3, with eight fins per row, provides intermediate gains, and Case 4, the smallest, establishing a monotonic trend versus fin density under constant row count.

As shown in Table 6, Case 5, with ten fins per row, had the largest fin surface area, which significantly contributed to its faster energy absorption and reduced melting time. The effective volume remained constant across the cases, because *EV* is constant for Cases 3–5, the performance differences isolate the effect of per-row area rather than convection allowance.

Table 4
Fins surface area, effective surface area of tube, and effective volume for cases 1, 2, and 3.

Case	Number of rows	Fins surface area (A_f) (mm^2)		Effective volume (EV) (mm^3)
		Total fin surface	Each row	
Case 1	3	2072	691	63434
Case 2	5	2639	528	42625
Case 3	8	3305	413	26312

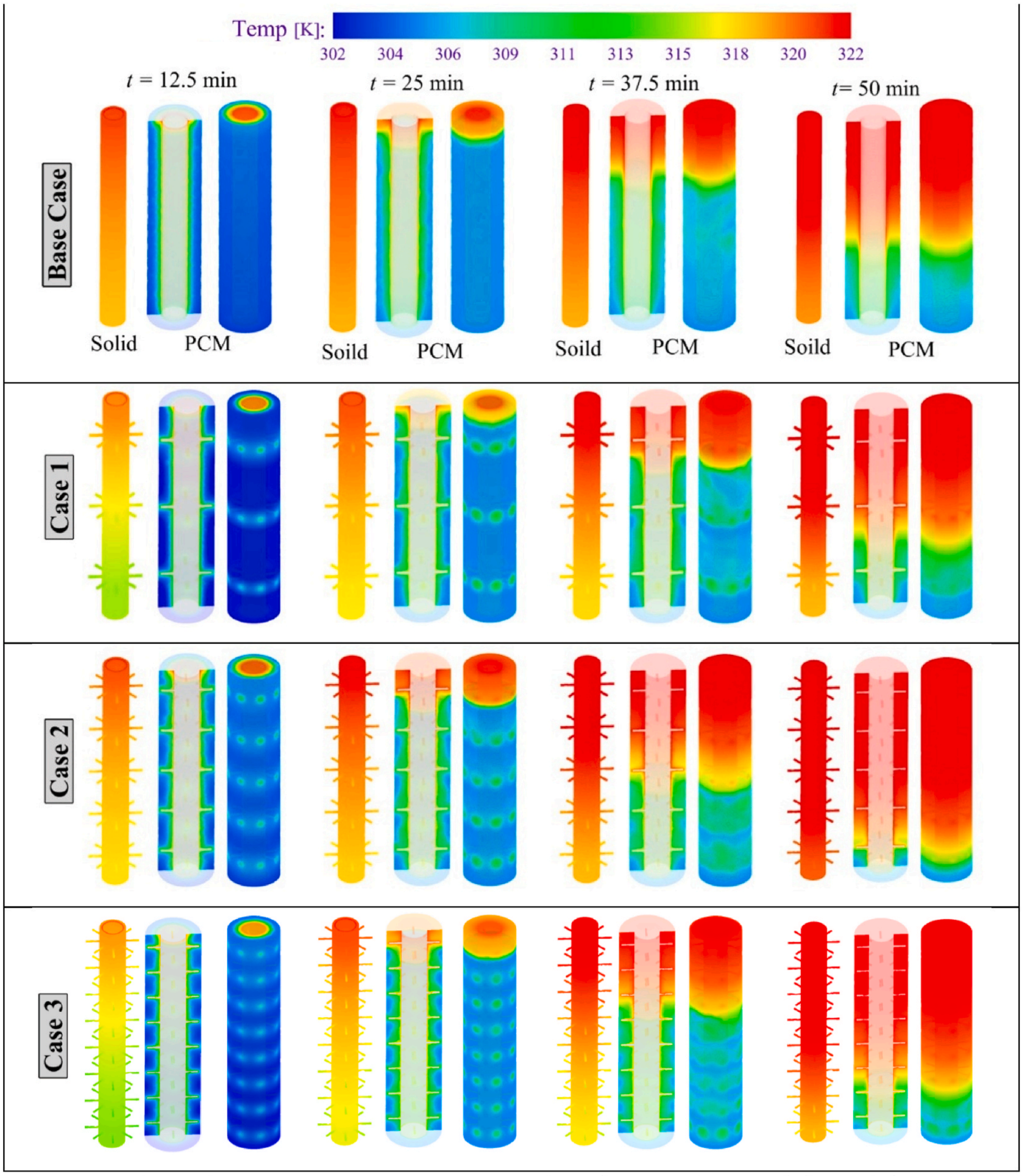

Fig. 9. Temperature contour comparison for Base Case and Cases 1-3.

Fig. 12 presents the temperature contours for the solid components (tube and fins) and the PCM, showing that Case 5 had the most uniform heat distribution. The broader warm regions and earlier disappearance of cold cores in Case 5 are consistent with its 24.6 % reduction in $t_{0.95}$ (Table 5). In short, when row spacing is fixed, higher fin density primarily boosts conduction and yields monotonic improvements in melt time.

6.3. Effect of staggered form

Fig. 13 illustrates the evolution of FMV and energy storage for cases where the fin arrangement was altered. The staggered configurations were explored in Cases 6–8, which feature five fins per row across sixteen rows, in comparison to Case 5, which has ten fins per row across eight rows. Despite the difference in row configuration, all cases maintain a total of eighty fins. The results indicate that, in addition to the number of rows, the arrangement of fins significantly affects both the amount of energy stored and the melting process.

In earlier sections, it was shown that increasing the number of fin rows can reduce the melting rate due to a decrease in convection heat transfer. This is because closely packed rows act as barriers to the flow of molten PCM, impeding its circulation. Conversely, increasing the number of fins per row enhances melting by increasing the surface area available for heat transfer. For instance, Case 5, with eight rows and ten fins per row, outperformed Case 6, which has sixteen rows and five fins per row, due to the reduced interference with natural convection in Case 5.

The primary objective of this section is to evaluate whether altering the placement of fins in Case 6 can improve performance by enhancing convection heat transfer. In Case 6, fins are uniformly aligned across all rows, while in Case 7, fins are positioned at specific angles relative to adjacent rows. Case 8 employs a staggered arrangement, where every third row is aligned with the first row, creating a repeating offset pattern. As shown in Fig. 13, the staggered configurations in Cases 7 and 8 demonstrate significant improvements in PCM melting and energy storage compared to Case 6. Specifically, Case 8 achieves the best performance, with a 27.9 % reduction in melting time compared to the Base Case, as detailed in Table 7. This indicates that modifying fin placement can effectively mitigate the adverse effects of additional rows on natural convection. Physically, staggering opens axial “chimneys” between successive rows, allowing buoyant plumes to traverse the array with less wake interference.

Fig. 14 provides a comparative analysis of the melting and temperature contours for Cases 6 and 8. For equal total fin area (Table 8), Case 8 shows earlier coalescence of high-FMV regions along the central plane and thicker hot layers near the outlet, confirming stronger, less-blocked convection than in the aligned Case 6.

Table 8 explains why arrangement matters despite identical A_{fT} with 16 rows, the per-row area in Cases 6–8 is only 230 mm^2, half that of Case 5 (10 × 8, 460 mm^2). Staggering compensates for this per-row deficit by restoring convection paths; thus Case 8 approaches the conduction benefit of high area while avoiding the convection penalty of perfect alignment.

All cases (5–8) have a total of 80 fins with the same shape, and as shown in Table 8, the total surface area of the fins in each case is identical, amounting to 3680 square millimeters. However, Case 5 has fewer rows compared to the other cases, resulting in a larger fin surface area per row. Consequently, Case 5 also has a greater effective surface area. Moreover, Table 8 shows a larger *EV* for Case 5 (26,364 mm^3) than for Cases 6–8 (13,748 mm^3), quantifying the additional convection allowance that helps Case 5 outperform the 16-row aligned case. As shown in Fig. 15, Case 8 exhibits more uniform heat transfer. Among the 16-row designs, the staggered Case 8 best balances area and convection, delivering the fastest melting within this subset (Table 7).

The observed balance between added surface area and preserved natural convection is consistent with established LHTES literature on pin-finned enclosures, where excessive finning can suppress buoyancy and lengthen the tail of melting, while staggered or sparse patterns maintain plume pathways and improve overall melt time. Reported optimal designs similarly combine moderate row counts with staggered phasing to maximize conduction without choking convection. Our results (optimum at 5 rows, best staggered pattern among 16-row layouts, and = 27.9 % improvement vs. Base) fall within the reported performance envelope for PCM-based systems of comparable scale [30,39,65].

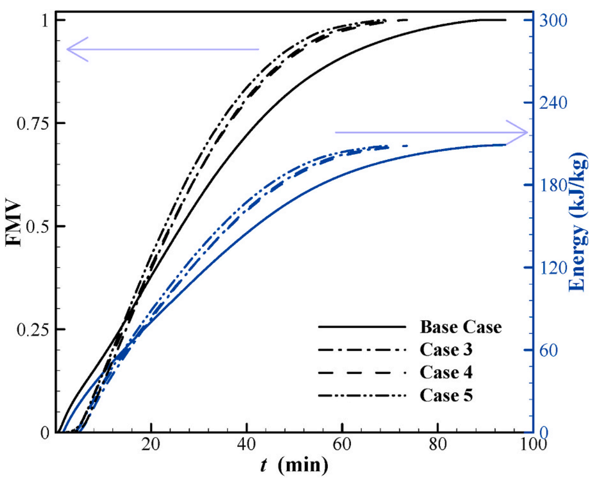

Fig. 10. A comparison of melting profiles for the Base Case (without fins), Case 3 (eight rows with eight fins per row), Case 4 (eight rows with six fins per row), and Case 5 (eight rows with ten fins per row).

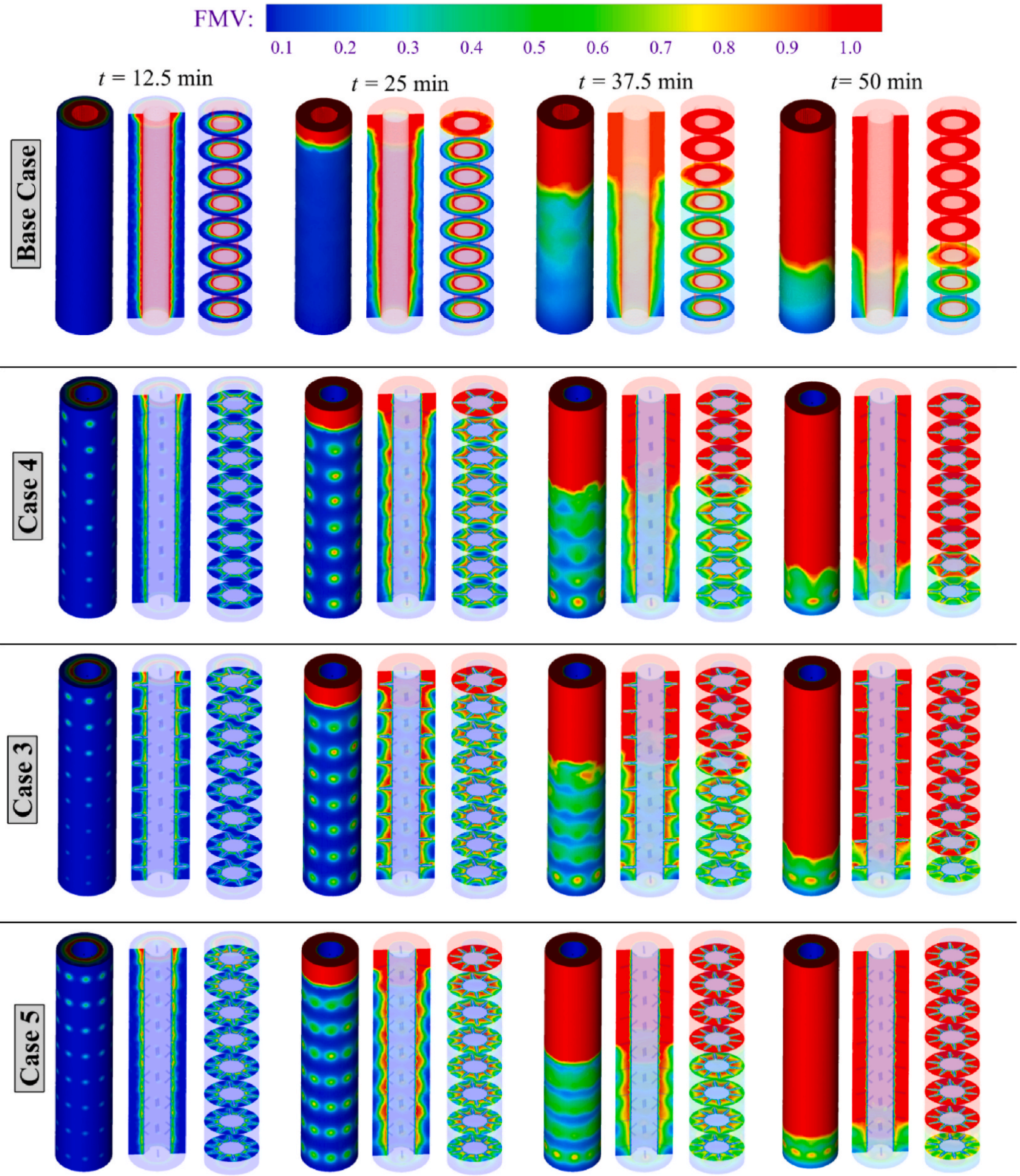

Fig. 11. FMV contour comparison for Base Case and Cases 3–5.

Table 5
Melting time comparison and percentage change in melting time for cases 3, 4, and 5 relatives to the Base Case across four amounts of FMV.

Case	Number of fins per row	FMV = 0.25		FMV = 0.5		FMV = 0.75		FMV = 0.95	
		t (min)	Time change (%)	*t* (min)	Time change (%)	*t* (min)	Time change (%)	*t* (min)	Time change (%)
Base Case	–	13.54	–	26.37	–	42.25	–	68.56	–
Case 4	6	14.24	5.2	24.07	−8.7	36.44	−13.8	55.06	−19.7
Case 3	8	14.78	9.1	24.24	−8.1	36.20	−14.3	54.03	−21.2
Case 5	10	13.69	1.1	22.87	−13.3	34.43	−18.5	51.73	−24.6

Table 6
Fins surface area, effective surface area of tube, and effective volume for cases 3, 4, and 5.

Case	Number of fins/row	Fins Surface Area (mm^2)		Effective Volume (mm^3)
		Total	Each row	
Case 4	6	2879	360	26235
Case 3	8	3305	413	26312
Case 5	10	3680	460	26364

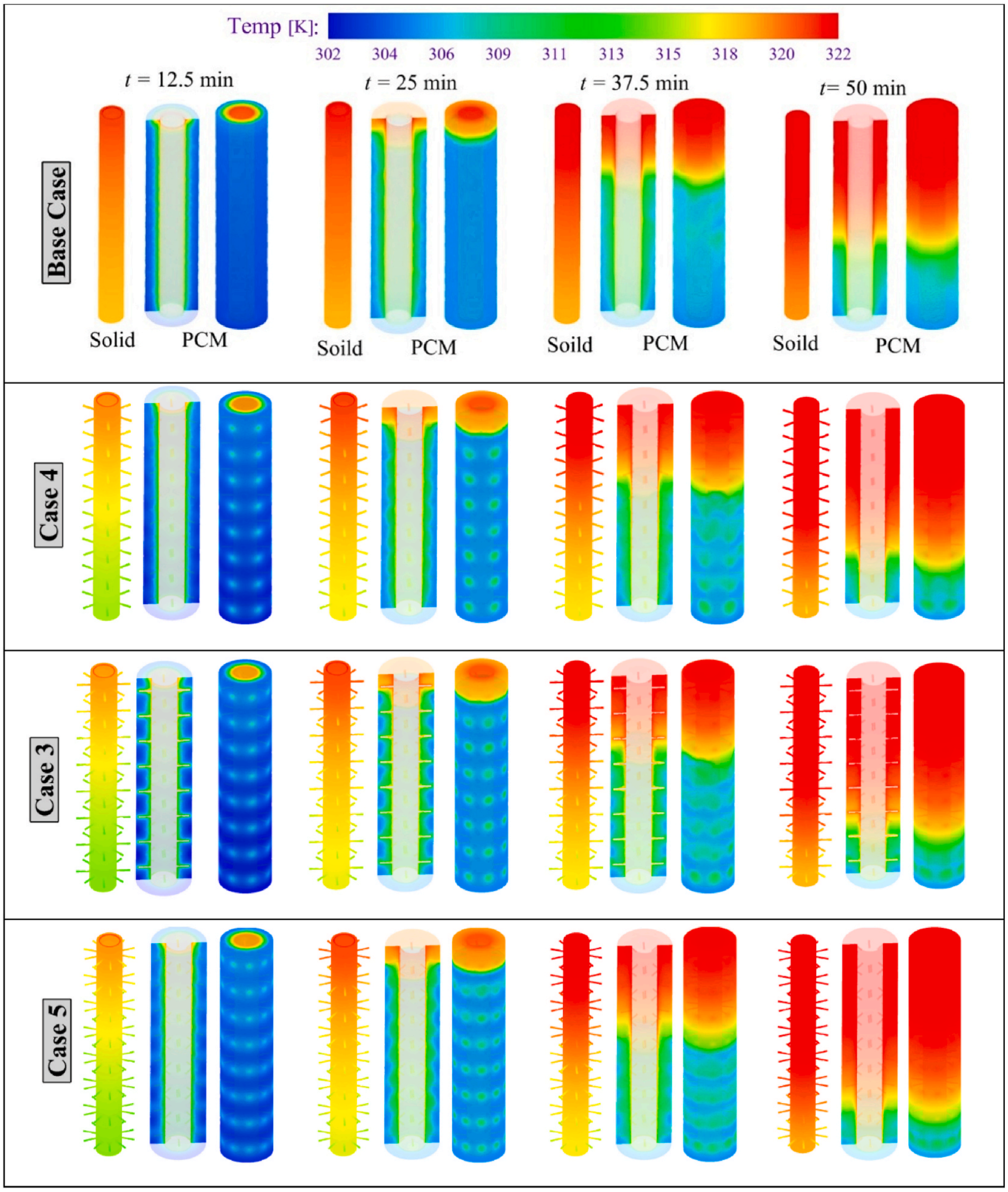

Fig. 12. Temperature contours comparison for Base Case and Cases 3–5.

6.4. *Comparison the cylindrical fins with disk fins*

To evaluate the performance of cylindrical and disk fins, a disk fin configuration (Cases 9) was designed, containing three fins, and

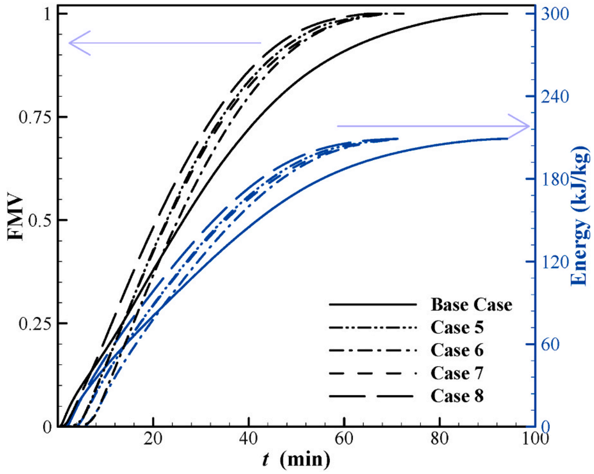

Fig. 13. Comparison of melting evolution profiles for Base Case (without fins).

Table 7
Melting time comparison and percentage change in melting time for cases 5–8 relatives to the Base Case across four amounts of FMV.

Case	FMV = 0.25		FMV = 0.5		FMV = 0.75		FMV = 0.95	
	t (min)	Time change (%)	*t* (min)	Time change (%)	*t* (min)	Time change (%)	*t* (min)	Time change (%)
Case 5	13.69	1.1	22.87	−13.3	34.43	−18.5	51.73	−24.6
Case 6	15.84	17.0	25.18	−4.5	37.01	−12.4	53.89	−21.4
Case 7	13.68	1.1	23.07	−12.5	35.07	−17.0	53.33	−22.2
Case 8	11.32	−16.4	20.74	−21.4	32.60	−22.8	49.44	−27.9

compared with the cylindrical fin configuration in Case 8, which demonstrated the best performance in previous tests. In Case 9, the disk thickness was set equal to the diameter of the cylindrical fins used in Case 8.

Fig. 16 shows the FMV and energy storage evolution during the PCM charging process for Cases 8 and 9. The results reveal that cylindrical fins (Case 8) outperform disk fins with equal thickness (Case 9) in both energy storage and melting efficiency. This indicates that when the thickness of disk and cylindrical fins is the same, cylindrical fins offer better overall performance.

As summarized in Table 9, Case 8 remained the top performer, while Case 9 achieved a 19.6 % decrease relative to the Base Case. Thus, pin fin arrangement of Case 8 is 10.2 % better than the disk fin Case 9. Fig. 17 presents the FMV contours for Cases 8 and 9 at various stages of melt processing. Despite the larger effective tube area reported for Case 9 (Table 10), the total fin area is substantially lower (1901 vs. 3680 mm^2), and the disks intermittently baffle the flow, fragmenting buoyant plumes (Fig. 17 b). In contrast, the slender cylindrical pins in Case 8 create continuous axial pathways that preserve plume coherence (Fig. 17 a). The much larger *EV* in Case 9 (63,434 mm^3) does not compensate for the reduced fin area and plume fragmentation, so conduction-limited heat transfer dominates and slows melting.

Fig. 18 shows the temperature contours for the PCM and solid components (fins and tube). Case 8 exhibits earlier warming of mid-height PCM and a thicker high-temperature layer near the outlet at each time stamp, consistent with its faster FMV evolution (Fig. 16).

In conclusion, cylindrical fins (Case 8) generally perform better than disk fins with equal thickness (Case 9), because they supply higher wetted area without creating strong baffles, thereby combining robust conduction with unobstructed buoyant circulation.

7. Conclusions

Using a strict equal-fin-volume framework, this study shows that geometry, not added material, sets the performance ceiling of finned LHTES: an intermediate row count and an optimal per-row density balance conduction gains against buoyancy preservation, staggered layouts open flow chimneys that cut melting time by 27.9 % versus no-fin and by 29 % versus inline arrays, and cylindrical (pin) fins outperform disk fins by 10.2 % because they maintain through-flow. These results yield practical design guidance for low-complexity thermal stores: (i) avoid over-crowding rows, (ii) tune per-row pin density to the convection pathway width, and (iii) prefer staggered pin arrays when natural convection is a key driver. The findings are derived from a 3-D numerical study and should be validated experimentally across PCM types and fin materials and assessed at scale in full-size units.

Re-shaping and re-positioning the fins increase charge and discharge power without adding fin mass or reducing the amount of phase-change material, so storage capacity is preserved. This is most useful for building thermal stores with daily cycling (walls, ceilings, domestic hot-water tanks), solar-thermal batteries with intermittent input, and industrial waste-heat recovery with short dwell times. For very long cycles focused mainly on total stored energy, the benefit is smaller.

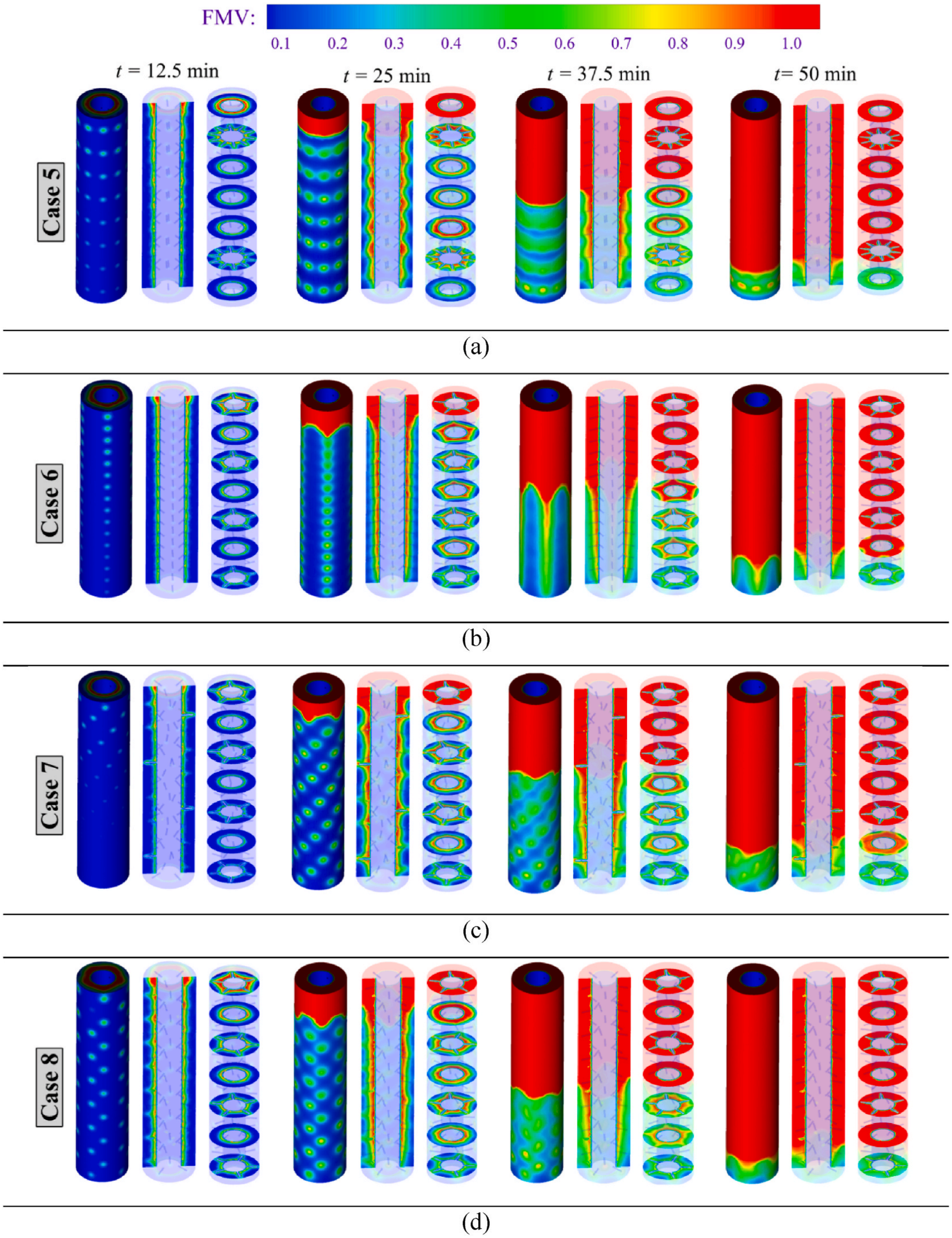

Fig. 14. FMV contour comparison for Case 5 (with 8 rows and ten fins in every row) and Cases 6–8 (with 16 rows and five fins in every row).

Table 8
Fins surface area, effective surface area of tube, and effective volume for cases 5–8.

Case	Fins Surface Area (mm^2)		Effective Volume (mm^3)
	Total	Each row	
Case 5	3680	460	26364
Case 6-8	3680	230	13748

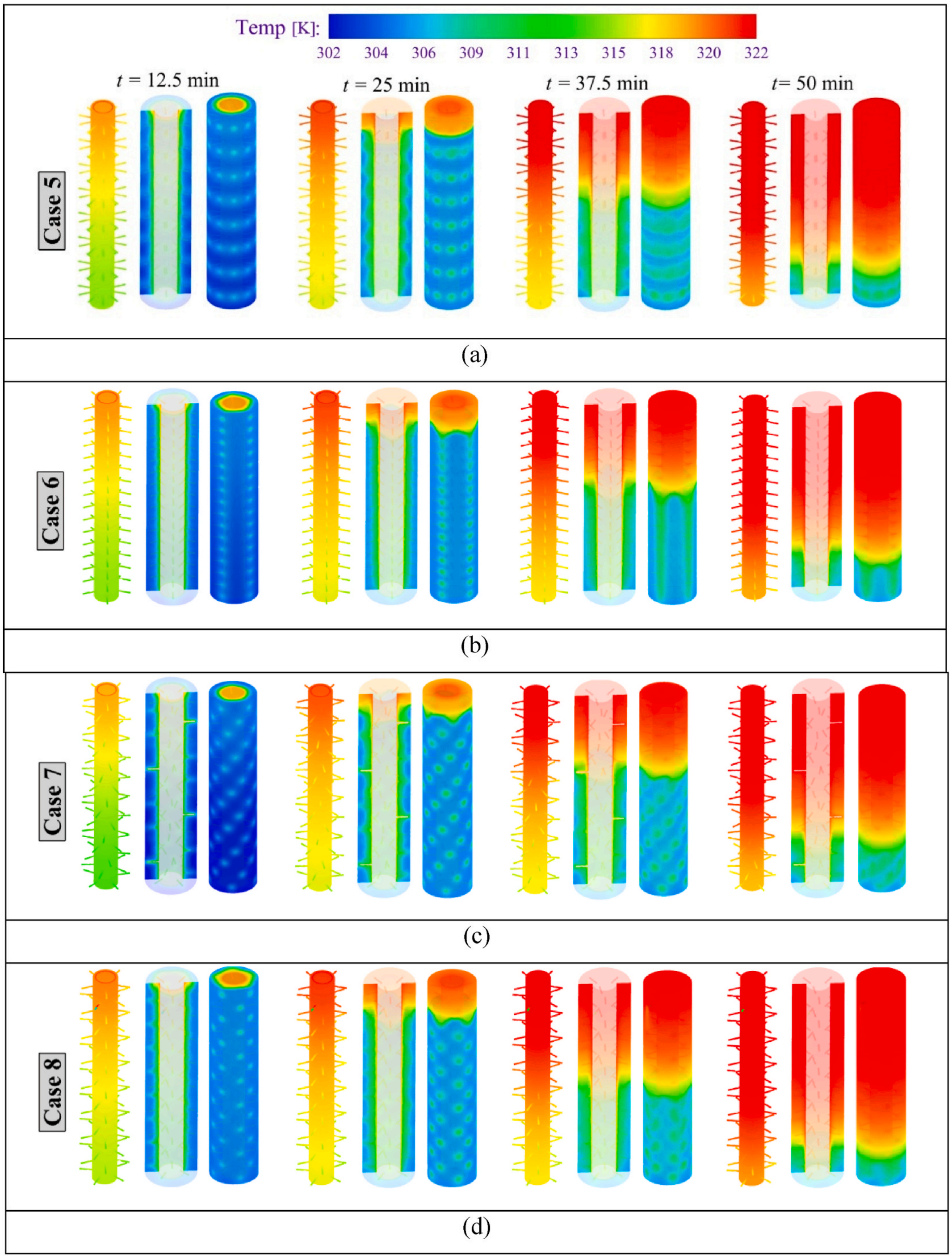

Fig. 15. Temperature contour comparison for Case 5 (with 8 rows and ten fins in every row) and Case 6 (with 16 rows and five fins in every row).

CRediT authorship contribution statement

Fathi Alimi: Writing – review & editing, Writing – original draft, Resources, Methodology, Investigation, Formal analysis, Data curation, Conceptualization. **Abdul Amir H. Kadhum:** Writing – original draft, Software, Resources, Investigation, Data curation, Conceptualization. **Mohamed Bouzidi:** Writing – original draft, Resources, Project administration, Methodology, Investigation, Data curation. **Mohammed Hasan Ali:** Writing – original draft, Visualization, Software, Methodology, Investigation, Formal analysis. **Hammadi Khmissi:** Writing – original draft, Investigation, Formal analysis, Data curation, Conceptualization. **Zehba Raizah:** Writing

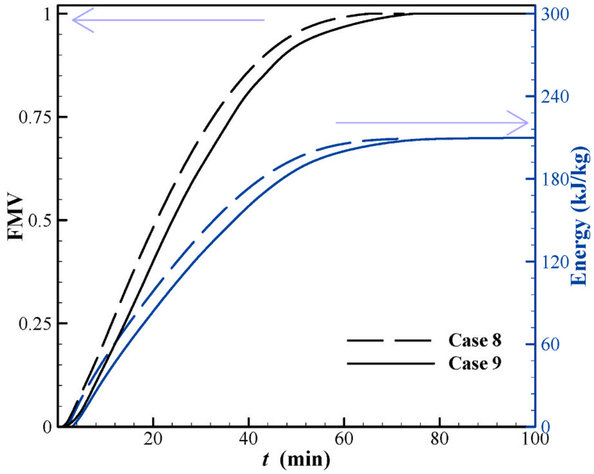

Fig. 16. Comparison of melting evolution profiles between the best fin case (Case 8), and the disk case with the thickness as equal the diameter of Case 8.

Table 9
Melting time comparison and percentage change relative to the base case.

Case	FMV = 0.25		FMV = 0.5		FMV = 0.75		FMV = 0.95	
	t (min)	Time change (%)	*t* (min)	Time change (%)	*t* (min)	Time change (%)	*t* (min)	Time change (%)
Case 8	11.32	−16.4	20.74	−21.4	32.60	−22.8	49.44	−27.9
Case 9	14.05	3.8	24.06	−8.8	36.45	−13.7	55.10	−19.6

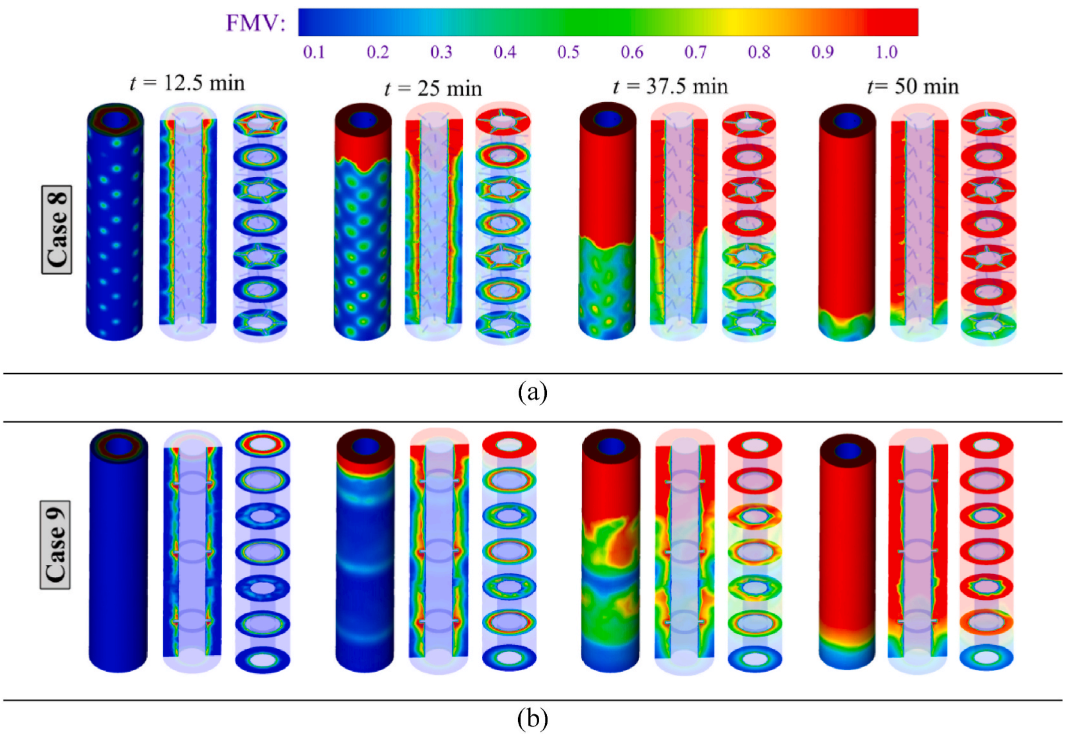

Fig. 17. FMV contour comparison for cases 8, and 9.

Table 10
Fins surface area, effective surface area of tube, and effective volume for cases 8, 9.

	Fins Surface Area (mm^2)		Effective Surface Area of Tube (mm^2)	Effective Volume (mm^3)
	Total	Each row		
Case 8	3680	230	739	13748
Case 9	1901	634	3142	63434

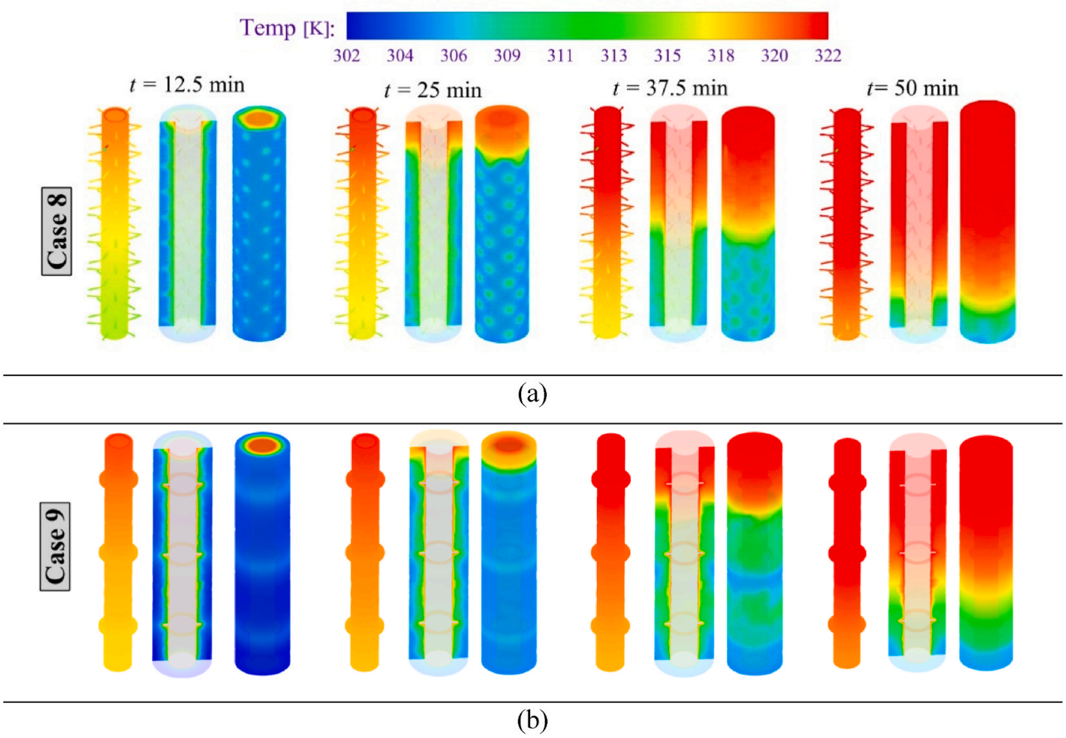

Fig. 18. Temperature contour comparison for Case 8 and Case 9.

– review & editing, Visualization, Methodology, Investigation, Funding acquisition, Formal analysis, Conceptualization. **Faisal Alresheedi:** Methodology, Investigation, Formal analysis, Conceptualization. **Turki Alkathiri:** Writing – original draft, Visualization, Formal analysis, Data curation. **D. Iranian:** Writing – review & editing, Writing – original draft, Validation, Supervision, Investigation, Formal analysis, Conceptualization.

Declaration of competing interest

The authors clarify that there is no conflict of interest for report.

Acknowledgments

The authors extend their appreciation to the Deanship of Research and Graduate Studies at King Khalid University for funding this work through large Research Group Project under the grant number (RGP2/395/46). The authors extend their appreciation to the Deanship of Scientific Research at Northern Border University, Arar, KSA for funding this research work through the project number "NBU-FPEJ-2025-2222-01".

Data availability

Data will be made available on request.

References

[1] A. Jaberi, S. Hossainpour, A. Kiyoumarsioskouei, The impact of utilizing porous fins on the performance of PCM melting process in a horizontal latent heat thermal energy storage, J. Energy Storage 97 (2024).
[2] Y. Zhao, J. Song, M. Liu, Y. Zhao, A.V. Olympios, P. Sapin, J. Yan, C.N. Markides, Thermo-economic assessments of pumped-thermal electricity storage systems employing sensible heat storage materials, Renew. Energy 186 (2022) 431–456.
[3] L. Liu, D. Su, Y. Tang, G. Fang, Thermal conductivity enhancement of phase change materials for thermal energy storage: a review, Renew. Sustain. Energy Rev. 62 (2016) 305–317.
[4] A.H.N. Al-Mudhafar, A.L. Tarish, Enhancing PCM melting in a triple tube heat exchanger by utilizing innovative fins configurations, J. Braz. Soc. Mech. Sci. Eng. 46 (5) (2024).
[5] X. Zheng, Y. Zhou, A three-dimensional unsteady numerical model on a novel aerogel-based PV/T-PCM system with dynamic heat-transfer mechanism and solar energy harvesting analysis, Appl. Energy 338 (2023).
[6] Q. Al-Yasiri, M. Szabó, Experimental study of PCM-enhanced building envelope towards energy-saving and decarbonisation in a severe hot climate, Energy Build. 279 (2023) 112680.
[7] K. Du, J. Calautit, P. Eames, Y. Wu, A state-of-the-art review of the application of phase change materials (PCM) in mobilized-thermal energy storage (M-TES) for recovering low-temperature industrial waste heat (IWH) for distributed heat supply, Renew. Energy 168 (2021) 1040–1057.
[8] X.-Y. Li, L. Yang, X.-L. Wang, X.-Y. Miao, Y. Yao, Q.-Q. Qiang, Investigation on the charging process of a multi-PCM latent heat thermal energy storage unit for use in conventional air-conditioning systems, Energy 150 (2018) 591–600.
[9] M. Ghalambaz, I. Pop, M. Sheremet, M.H. Ali, M. Ghalambaz, Numerical and artificial neural network analysis of magnetohydrodynamic natural convection in a nano-encapsulated phase change suspension filled quadrantal circular enclosure, J. Appl. Comput. Mech. 11 (4) (2025) 929–945.
[10] J. Shafi, O. Younis, S. Tiari, M. Ghalambaz, Artificial intelligence–numerical study of melting and solidification heat transfer in a bundle of petal tubes embedded in metal foam, Appl. Therm. Eng. (2025) 127960.
[11] S. Al Arni, H.S.S. Aljibori, H.M. Mehdi, F. Gamaoun, J.M. Mahdi, P. Talebizadehsardari, N.B. Khedher, An efficient approach for latent heat storage: novel system design with wavy interconnecting fins and dual-mode operation, J. Energy Storage 138 (2025) 118652.
[12] N.S. Dhaidan, A.F. Hassan, A.M. Rasheed Al-Gaheeshi, F.N. Al-Mousawi, R.Z. Homod, Experimental investigation of thermal characteristics of phase change material in finned heat exchangers, J. Energy Storage 71 (2023).
[13] Q. Mao, X. Hu, T. Li, Study on heat storage performance of a novel vertical shell and multi-finned tube tank, Renew. Energy 193 (2022) 76–88.
[14] Q. Mao, Y. Li, G. Li, A. Badiei, Study on the influence of tank structure and fin configuration on heat transfer performance of phase change thermal storage system, Energy 235 (2021) 121382.
[15] F. ul Hasnain, M. Irfan, M.M. Khan, L.A. Khan, H.F. Ahmed, Melting performance enhancement of a phase change material using branched fins and nanoparticles for energy storage applications, J. Energy Storage 38 (2021) 102513.
[16] S. Yao, X. Huang, Study on solidification performance of PCM by longitudinal triangular fins in a triplex-tube thermal energy storage system, Energy 227 (2021).
[17] N. Modi, X. Wang, M. Negnevitsky, F. Cao, Melting characteristics of a longitudinally finned-tube horizontal latent heat thermal energy storage system, Sol. Energy 230 (2021) 333–344.
[18] M. Ahmadian-Elmi, A. Mashayekhi, S. Nourazar, K. Vafai, A comprehensive study on parametric optimization of the pin-fin heat sink to improve its thermal and hydraulic characteristics, Int. J. Heat Mass Tran. 180 (2021) 121797.
[19] A.M. Ranjbar, Z. Pouransari, M. Siavashi, Improved design of heat sink including porous pin fins with different arrangements: a numerical turbulent flow and heat transfer study, Appl. Therm. Eng. 198 (2021) 117519.
[20] A.A. Sertkaya, M. Ozdemir, E. Canli, Effects of pin fin height, spacing and orientation to natural convection heat transfer for inline pin fin and plate heat sinks by experimental investigation, Int. J. Heat Mass Tran. 177 (2021) 121527.
[21] J. Duan, Y. Xiong, D. Yang, Study on the effect of multiple spiral fins for improved phase change process, Appl. Therm. Eng. 169 (2020) 114966.
[22] B. Lu, Y. Zhang, D. Sun, Z. Yuan, S. Yang, Experimental investigation on thermal behavior of paraffin in a vertical shell and spiral fin tube latent heat thermal energy storage unit, Appl. Therm. Eng. 187 (2021) 116575.
[23] D.S. Mehta, B. Vaghela, M.K. Rathod, J. Banerjee, Thermal performance augmentation in latent heat storage unit using spiral fin: an experimental analysis, J. Energy Storage 31 (2020) 101776.
[24] C. Yu, S. Wu, Y. Huang, F. Yao, X. Liu, Charging performance optimization of a latent heat storage unit with fractal tree-like fins, J. Energy Storage 30 (2020) 101498.
[25] I. El Ghandouri, A. El Maakoul, S. Saadeddine, M. Meziane, Thermal performance of a corrugated heat dissipation fin design: a natural convection numerical analysis, Int. J. Heat Mass Tran. 180 (2021) 121763.
[26] Y. Huang, D. Cao, D. Sun, X. Liu, Experimental and numerical studies on the heat transfer improvement of a latent heat storage unit using gradient tree-shaped fins, Int. J. Heat Mass Tran. 182 (2022) 121920.
[27] C. Zhang, Y. Huang, Y. Chen, Bionic study on latent heat thermal storage, Renew. Sustain. Energy Rev. 183 (2023) 113529.
[28] M.K. Rathod, J. Banerjee, Thermal performance enhancement of shell and tube latent heat storage unit using longitudinal fins, Appl. Therm. Eng. 75 (2015) 1084–1092.
[29] Y. Yuan, X. Cao, B. Xiang, Y. Du, Effect of installation angle of fins on melting characteristics of annular unit for latent heat thermal energy storage, Sol. Energy 136 (2016) 365–378.
[30] Y. Zhang, B. Sun, X. Zheng, P.K. Singh, H. Ayed, A. Mouldi, A. Mohamed, S. Mehrez, Investigation on effect of connection angle of "L" shaped fin on charging and discharging process of PCM in vertical enclosure, Case Stud. Therm. Eng. 33 (2022).
[31] S. Tiari, A. Hockins, K. Shank, Experimental study of a latent heat thermal energy storage system assisted by varying annular fins, J. Energy Storage 55 (2022).
[32] R. De Césaro Oliveski, F. Becker, L.A.O. Rocha, C. Biserni, G.E.S. Eberhardt, Design of fin structures for phase change material (PCM) melting process in rectangular cavities, J. Energy Storage 35 (2021).
[33] S.D. Farahani, A.D. Farahani, E. Hajian, H.F. Öztop, Control of PCM melting process in an annular space via continuous or discontinuous fin and non-uniform magnetic field, J. Energy Storage 55 (2022).
[34] Y. Huang, H. Zhai, Z. Deng, A novel elastic-driven phase-change thermal buffer for efficient thermal management, Int. J. Heat Mass Tran. 239 (2025) 126586.
[35] Y. Huang, C. Zhang, Y. Chen, Rapid charging and discharging strategies for latent heat storage, Renew. Sustain. Energy Rev. 222 (2025) 115953.
[36] R. Zhu, D. Jing, Numerical study on thermal and melting performances of a horizontal latent heat storage unit with branched tree-like convergent fins, J. Energy Storage 62 (2023).
[37] B. Huang, S. Yang, X. Li, J. Wang, P.D. Lund, Strengthening of melting-solidification process in latent heat storage through sine wave shaped fins, J. Energy Storage 66 (2023).
[38] F. Alimi, H.S.S. Aljibori, M. Bouzidi, A. Alasmari, S. Yazdani, M. Ghalambaz, Improving a shell-tube latent heat thermal energy storage unit for building hot water demand using metal foam inserts at a constant pumping power, J. Build. Eng. 98 (2024) 111040.
[39] F. Liu, G. Zhang, Study on melting and solidification performances improvement of phase change material using novel branch fin structure, J. Energy Storage 63 (2023).
[40] K. Shank, J. Bernat, Q. Justice, P. Niksiar, S. Tiari, Experimental study of a latent heat thermal energy storage system assisted by variable-length radial fins, J. Energy Storage 68 (2023).
[41] Y. Xu, C. He, Y. Chen, Y. Sun, H. Yin, Z.-J. Zheng, Experimental and numerical study on the effect of the intelligent memory metal fin on the melting and solidification process of PCM, Renew. Energy 218 (2023).
[42] L. Wang, Y. Lei, B. Du, Y. Li, J. Sun, Performance enhancement of a horizontal latent thermal energy storage unit with elliptical fins, Appl. Therm. Eng. 225 (2023).

[43] S. Baghaei Oskouei, Ö. Bayer, Experimental and numerical investigation of melting and solidification enhancement using Fibonacci-inspired fins in a latent thermal energy storage unit, Int. J. Heat Mass Tran. 210 (2023).
[44] M. Gürtürk, B. Kok, A new approach in the design of heat transfer fin for melting and solidification of PCM, Int. J. Heat Mass Tran. 153 (2020).
[45] Q. Mao, Y. Zhu, T. Li, Heat storage performance of PCM in a novel vertical pointer-shaped finned latent heat tank, J. Therm. Sci. 33 (2) (2024) 422–434.
[46] S.-K. Choi, S.-O. Kim, T.-H. Lee, Dohee-Hahn, Computation of the natural convection of nanofluid in a square cavity with homogeneous and nonhomogeneous models, Numer. Heat Transf. A Appl. 65 (4) (2014) 287–301.
[47] A. Agarwal, R. Sarviya, Characterization of commercial grade paraffin wax as latent heat storage material for solar dryers, Mater. Today Proc. 4 (2) (2017) 779–789.
[48] N.B. Khedher, H. Togun, A.M. Abed, H.M.T. Al-Najjar, A. Dulaimi, H.I. Mohammed, J.M. Mahdi, A. Yvaz, P. Talebizadehsardari, Discharge performance assessment of a vertical double-pipe latent heat storage unit equipped with circular Y-shaped fins, J. Build. Eng. 75 (2023) 106870.
[49] H. Zheng, C. Wang, Q. Liu, Z. Tian, X. Fan, Thermal performance of copper foam/paraffin composite phase change material, Energy Convers. Manag. 157 (2018) 372–381.
[50] N.B. Khedher, H.I. Mohammed, A.M. Abed, N. Biswas, H. Togun, K.A. Hammoodi, J.M. Mahdi, P. Talebizadehsardari, Maximizing charging/discharging capabilities of horizontal shell-and-tube latent heat storage systems with innovative curved fin inserts, Int. J. Heat Mass Tran. 236 (2025) 126289.
[51] M. Benaissa, H.S.S. Aljibori, A.M. Abed, J.M. Mahdi, H.I. Mohammed, O. Younis, P. Talebizadehsardari, N.B. Khedher, Maximizing thermal response in latent heat thermal energy storage systems: a comprehensive study of wavy fin configuration and distribution, Int. Commun. Heat Mass Tran. 159 (2024) 108172.
[52] M.A. Said, H.S.S. Aljibori, J.M. Mahdi, H.I. Mohammed, P. Talebizadehsardari, A. Keshmiri, Modifying the performance kinetics in the shell-and-multi tube latent heat storage system via dedicated finned tubes for building applications, J. Build. Eng. 97 (2024) 110722.
[53] N.S. Bondareva, M.A. Sheremet, Natural convection melting influence on the thermal resistance of a brick partially filled with phase change material, Fluids 6 (7) (2021) 258.
[54] J. Blazek, Principles of solution of the governing equations, in: J. Blazek (Ed.), Computational Fluid Dynamics: Principles and Applications, third ed., 2015, pp. 121–166.
[55] P. Wang, X. Wang, Y. Huang, C. Li, Z. Peng, Y. Ding, Thermal energy charging behaviour of a heat exchange device with a zigzag plate configuration containing multi-phase-change-materials (m-PCMs), Appl. Energy 142 (2015) 328–336.
[56] N.B. Khedher, K. Hosseinzadeh, A.M. Abed, K. Khosravi, J.M. Mahdi, H.S. Sultan, H.I. Mohammed, P. Talebizadehsardari, Accelerated charging of PCM in coil heat exchangers via central return tube and inlet positioning: a 3D analysis, Int. Commun. Heat Mass Tran. 152 (2024) 107275.
[57] M. Esapour, M. Hosseini, A. Ranjbar, Y. Pahamli, R. Bahrampoury, Phase change in multi-tube heat exchangers, Renew. Energy 85 (2016) 1017–1025.
[58] S. Mat, A.A. Al-Abidi, K. Sopian, M.Y. Sulaiman, A.T. Mohammad, Enhance heat transfer for PCM melting in triplex tube with internal–external fins, Energy Convers. Manag. 74 (2013) 223–236.
[59] W.-B. Ye, D.-S. Zhu, N. Wang, Numerical simulation on phase-change thermal storage/release in a plate-fin unit, Appl. Therm. Eng. 31 (17) (2011) 3871–3884.
[60] E. Assis, L. Katsman, G. Ziskind, R. Letan, Numerical and experimental study of melting in a spherical shell, Int. J. Heat Mass Tran. 50 (9) (2007) 1790–1804.
[61] B. Kamkari, H. Shokouhmand, F. Bruno, Experimental investigation of the effect of inclination angle on convection-driven melting of phase change material in a rectangular enclosure, Int. J. Heat Mass Tran. 72 (2014) 186–200.
[62] A. Arshad, H.M. Ali, S. Khushnood, M. Jabbal, Experimental investigation of PCM based round pin-fin heat sinks for thermal management of electronics: effect of pin-fin diameter, Int. J. Heat Mass Tran. 117 (2018) 861–872.
[63] M.Z. Mahmoud, H.I. Mohammed, J.M. Mahdi, D.O. Bokov, N. Ben Khedher, N.K. Alshammari, P. Talebizadehsardari, W. Yaïci, Melting enhancement in a triple-tube latent heat storage system with sloped fins, Nanomaterials 11 (11) (2021) 3153.
[64] V. Safari, B. Kamkari, N. Hewitt, K. Hooman, Experimental comparative study on thermal performance of latent heat storage tanks with pin, perforated, and rectangular fins at different orientations, Therm. Sci. Eng. Prog. 48 (2024) 102401.
[65] R. Triki, S. Chtourou, M. Baccar, Heat transfer enhancement of phase change materials PCMs using innovative fractal H-shaped fin configurations, J. Energy Storage 73 (2023).